Am J Transl Res 2021;13(10):11501-11512
www.ajtr.org /ISSN:1943-8141/AJTR0133527

Original Article

Metabolic and biophysical study of the MFN2^{Ile213Thr} mutant causing Hereditary Motor and Sensory Neuropathy (HMSN)

Kai Yang[1*], Hua-Ying Hu[2*], Jing Zhang[3*], You-Sheng Yan[1], Wen-Qi Chen[3], Yan Liu[1], Yong-Qing Sun[1], Qing Guo[3], Cheng-Hong Yin[1]

[1]Prenatal Diagnosis Center, Beijing Obstetrics and Gynecology Hospital, Capital Medical University, Beijing, China; [2]Jiaen Genetics Laboratory, Beijing Jiaen Hospital, Beijing 100191, China; [3]Prenatal Diagnosis Center, Shijiazhuang Obstetrics and Gynecology Hospital, Shijiazhuang, Hebei, China. [*]Equal contributors.

Received March 25, 2021; Accepted July 30, 2021; Epub October 15, 2021; Published October 30, 2021

Abstract: Charcot-Marie-Tooth (CMT) 2A disease, a genetic axonal nervous lesion, results from *MFN2* pathogenic variation, and this gene plays a pivotal role in mitochondrial dynamics and calcium signaling. However, the underlying mechanism linking MFN2 defect to progressive dying-back of peripheral nerves is still unclear. The present work focused on analyzing one CMT2A patient from multiple perspectives. Clinical and pathologic evaluation was initially conducted on the recruited case. Subsequently, Sanger sequencing and whole-exome sequencing (WES) were performed for genetic detection. To reveal the cell metabolic alteration caused by the identified variant, this study also established and transfected plasmid vectors in HEK293 cells and analyzed cell metabolites through liquid chromatography in combination with quadrupole time-of-flight tandem mass spectrometry (UPLC Q-TOF MS). Additionally, we completed structural modeling and molecular dynamic (MD) simulation to investigate the intramolecular impact of the variant. According to our results, the clinical and neuropathologic manifestations of the proband matched with the diagnosis of CMT. The causative variant *MFN2*: c.638T>C: (p.Ile213Thr) was identified through genetic analysis. Moreover, metabolic pathway enrichment results demonstrated that this variant significantly affected the metabolism of sphingolipids and glycerophospholipids. MD analysis indicated that this variant crippled the binding ability of MFN2 to GTP. Taken together, our study deduced preliminary clues for the underlying mechanism by which mutant MFN2 affects cell metabolism and provided a novel perspective to understand the cellular and molecular impacts of MFN2 variants.

Keywords: CMT2A, *MFN2*, hereditary neuropathy, whole-exome sequencing, molecular dynamic simulation, metabonomics

Introduction

HMSN (Hereditary motor and sensory neuropathy), also called Charcot-Marie-Tooth (CMT) disorder, was first depicted by 3 neurologists Howard Henry Tooth, Jean-Martin Charcot, and Pierre Marie as a “progressive muscle atrophy” in 1886. This is a heterogeneous disease characterized by progressive myasthenia of limbs [1, 2]. This syndrome is broadly classified as demyelinating (CMT1), intermediate, and axonal (CMT2) types [3], which involves nearly 100 genes. Typically, more than 80% of the cases result from *MPZ*, *GJB1,* and *MFN2* sequence mutations or *PMP22* copy number variation (CNV) [1, 4]. There is a certain degree of phenotypic overlap between different subtypes of CMT, or between CMT and other neurodegenerative diseases, making it challenging to make a phenotypic differential diagnosis [1, 3].

CMT2, the axonal form, causes more lower extremity involvement compared with upper extremities, involvement of distal upper extremity with the progression of disease, serious motor deficits compared with sensory deficits, along with mildly reduced or normal (>42 m/s) nerve conduction velocities (NCVs) [5]. About 1/3 of CMT2 patients who have a corresponding family history harbor an *MFN2* pathogenic

variant, which is recognized as CMT2A [5, 6]. Züchner *et al.* verified *MFN2* as the causative gene of CMT2A in 2004 [7]. Since then, over 200 pathogenic variants were discovered in *MFN2* gene based on The Human Gene Mutation Database (http://www.hgmd.cf.ac.uk/ac/index.php). Nevertheless, the genotype-phenotype correlation of this disorder is just preliminarily discussed, and is ascribed to the lack of in-depth investigation on large cohorts [8, 9], and the incomplete elucidation of the structural and functional properties of MFN2 [10, 11]. Thus, it remains challenging to define the precise mechanism connecting abnormal mitochondria with the progressive peripheral extremity nerve dying-back in CMT2A [11].

MFN2 gene (MIM *608507) is located on chromosome 1p36.22 and encodes the mitochondrial outer membrane GTPase, mitofusin2, which regulates the dynamics of mitochondria such as fission, fusion transportation, mitophagy, and the contact between mitochondria and other organelles [11-14]. Chen *et al.* demonstrated that the normal function of MFN2 was essential for the embryonic development in mice [14], and it protected from cerebellar neurodegeneration [15]. Bach *et al.* indicated that MFN2 expression was positively correlated with insulin sensitivity, and the modulation of MFN2 further regulated muscle metabolism [16]. Besides, a recent study suggests that MFN2 contributes to the metabolic regulation during the aging of chondrocytes *in vitro* [17]. However, it remains largely unclear about how MFN2, especially its mutants, affects the overall metabolic profile of cells and thus contributes to pathophysiologic processes.

At present, details regarding the specific spatio-temporal structure of MFN2 involved in mitochondrial dynamics are lacking, yet advances in the investigation of MFN2 protein structure have contributed to the understanding of its special functional conformations [18], pathogenesis [10], and the development of a therapeutic strategy [19, 20].

In the present study, a family suffering from HMSN was recruited for comprehensive neuropathologic and genetic diagnosis. A study strategy was generated in two directions according to the results. In one aspect, an expression vector carrying mutant *MFN2* cDNA was constructed and transfected into HEK-293 cells to discover its impact on cellular metabolic profile. In another, molecular dynamic (MD) analysis was performed to reveal the sub-molecular structural variation of the mutant MFN2 and its biologic effects.

Materials and methods

The Ethics Committee of Shijiazhuang Obstetrics and Gynecology Hospital approved our study protocols (approval no. 20200042). Each participant provided written informed consent for participation.

Subjects and clinical evaluation

A 33-year-old pregnant woman with a history of HMSN was admitted into the Prenatal Diagnosis Center of Shijiazhuang Obstetrics and Gynecology Hospital. The patient underwent a detailed medical history inquiry and clinical examination. Besides, the neuropathologic examination was also carried out on the patient based on the clinical situation. Further, all associated members in this family were recruited for clinical and genetic evaluation. A gastrocnemius nerve biopsy was also performed, and the sample was examined by scanning electron microscopy (SEM).

Genetic analysis

We collected peripheral blood (200 μl, for adults) and amniotic fluid (10 ml, for fetuses) from each participant, and then isolated genomic DNA by the use of DNA Blood Midi/Mini kit (Qiagen GmbH) in line with specific instructions. To detect genome-wide CNVs, chromosomal microarray analysis (CMA) using the SNP-array strategy (Cytoscan 750k, Affymetrix, USA) was conducted on the sample collected from the proband according to the manufacturer's protocols.

This study conducted whole-exome sequencing (WES) according to previous description [21]. Briefly, IDT's xGenExome Research Panel (Integrated DNA Technologies, San Diego, USA) was utilized to hybridize and capture DNA fragments. Later, QF-PCR (Quantitative Fluorescence PCR (QF-PCR)) was carried out to test all libraries, whereas Agilent Bioanalyzer 2100 (Agilent Technologies, Santa Clara, CA, USA) was utilized to determine content and size distribution. The pair-end reads (150 bp) were

adopted in DNA (~300 pM per sample) genomic sequencing by adopting the Novaseq6000 platform (Illumina, San Diego, USA) and the Novaseq Reagent Kit (https://www.illumina.com). Afterwards, we utilized the Burrows-Wheeler Aligner tool to align raw reads (quality level, Q30%>89%) into the human reference genome (accession no. hg19/GRCh37,ftp://hgdownload.cse.ucsc.edu/goldenPath/hg19/chromosomes/). Later, Picard v1.57 (http://picard.sourceforge.net/) was employed to remove PCR duplicates. Subsequently, Genome Analysis Toolkit (https://software.broadinstitute.org/gatk/) and Verita Trekker® Variants Detection system (v 2.0, Berry Genomics, Inc.) were utilized for variant calling. According to the American College of Medical Genetics and Genomics (ACMG) guidelines [23], variant annotation and interpretation were completed by Enliven® Variants Annotation Interpretation systems (Berry Genomics, Inc.) and ANNOVAR (v 2.0) [22].

Further, Sanger sequencing was performed as the validation method for suspected variations. MEGA7 (http://www.megasoftware.net) was employed to analyze the conservatism of those amino acids (AA) affected by missense variants using default parameters.

Plasmid construction, cell culture, and transfection

To further explore the functional impact on the cell metabolic level of the variant detected in this study, we constructed the expression plasmid vectors using the lentiviral vector (pLV-hef1a-mNeongreen-P2A-Puro-WPRE-CMV-MCS-3× flag) containing the wild-type (WT) or mutant (Mut, with variant c.638T>C) *MFN2* cDNA (detailed data shown in Supplementary Material 1).

HEK-293 cells were obtained commercially (SyngenTech Inc., Beijing, China) and cultured through regular means with DMEM supplemented with 10% BSA (Invitrogen, USA). Thereafter, the plasmid vectors were transfected into cells using Lipofectamine 2000 (ThermoFisher, USA). 48 h later, GFP intensity was observed under the fluorescence microscope and MFN2 expression was detected by QF-PCRto determine the transfection efficiency (detailed method shown in Supplementary Material 1).

Metabonomic analysis by liquid chromatography-mass spectrometry (LC-MS)

Later, the transfected cells were submitted to metabonomic analysis. The Nexera X2 system (Shimadzu, Japan) was utilized for ultra-performance liquid chromatography in combination with quadrupole time-of-flight tandem mass spectrometry (UPLC Q-TOF MS) using the Triple TOF 5600 quadrupole-time-of-flight mass spectrometer (AB SCIEX, USA). Afterwards, LC was carried out using the ZORBAX Eclipse Plus C18 column (2.1×100 mm, 3.5 um, Agilent, USA) kept under 45°C. MarkerView 1.2.1 and independent reference lock-mass ions through Analyst TF 1.6 were adopted for ensuring mass accuracy in the process of data collection. Then, the HMDB (http://www.hmdb.ca/spectra/ms/search) database was searched to identify those modified metabolite ions assigned, at a 0.05 Da mass tolerance.

Statistical analysis

Mann-Whitney U test was first conducted to compare the WT (No. pHS-AVC-LY059) group with Mut (No. pHS-AVC-LY 060) group. Distributions were determined by orthogonal projection to latent structure-discriminant analysis (PLS-DA); differences in metabolism of both groups were found through MetaboAnalyst 5.0 (http://www.metaboanalyst.ca/MetaboAnalyst/). Using the 10-fold approach and unit variance scaling, cross-validation of PLS-DA models was completed. With regard to PLS-DA models, we utilized parameter R2 for evaluating fitting condition, and used Q2 for assessing the prediction performance. An extremely low or negative Q2 value represented insignificant difference of both groups. In the PLS-DA models, variations in X matrix not related to Y matrix were eliminated. Therefore, just 1 predicting component was adopted to discriminate the 2 classes.

Pathway analysis

This study adopted MetaboAnalyst web portal for pathway analysis and visualization (http://www.metaboanalyst.ca/) to analyze chemical metabolites. We assessed the associations of metabolites through Pearson correlation analysis (significance levels: impact >0.01, $P<0.05$).

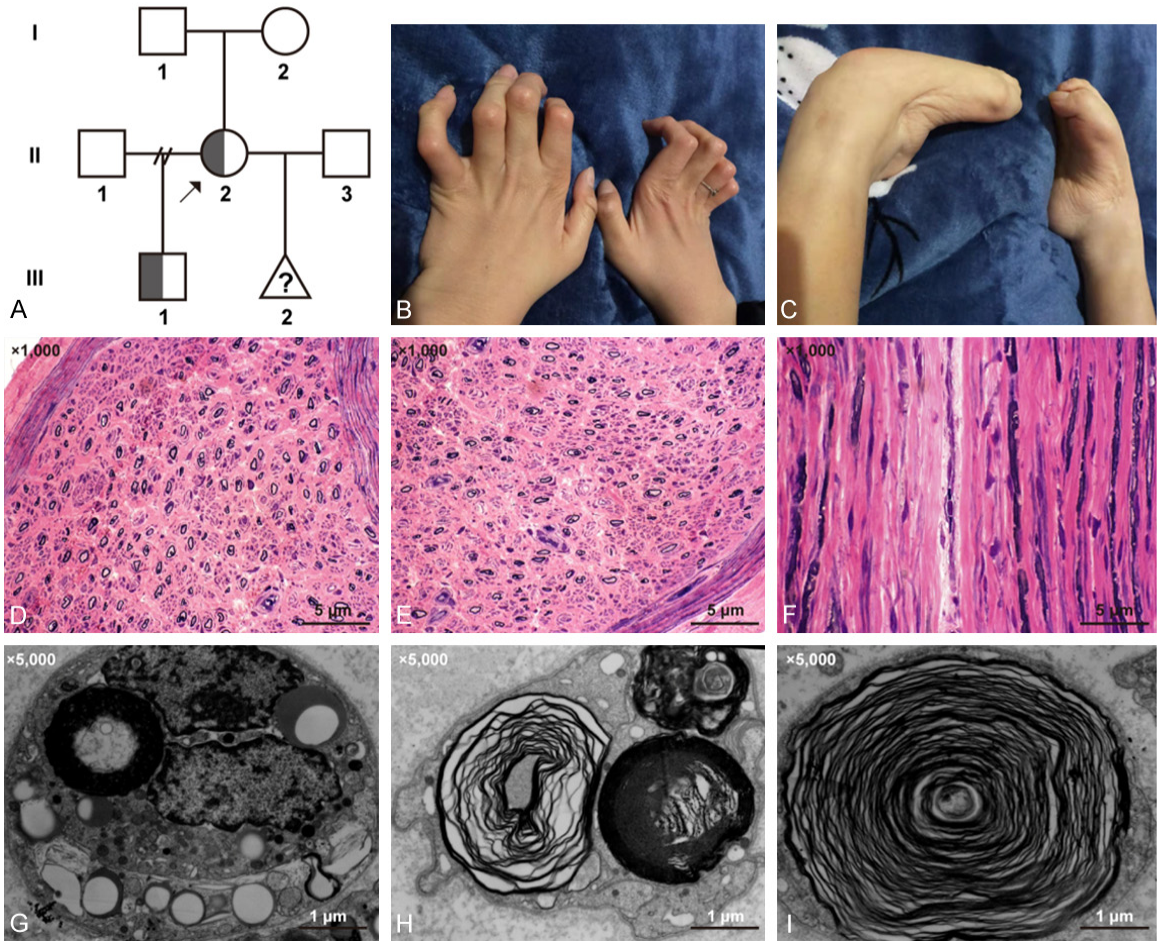

Figure 1. (A) Pedigree diagram of the affected family. II-2 was the pregnant proband with an affected son (III-1). The (B) hands and (C) feet of the proband. (D-F) Hematoxylin-eosin staining of the gastrocnemius nerve sample of the proband showing severe loss of myelinated nerve fibers. (Scale bar, 5 μ; (magnification: ×1000)). (G-I) Formation of numerous "onion bulbs" shown by scanning electron microscopy. (Scale bar, 1 μ; (magnification: ×5000)).

Structural modeling and molecular dynamic (MD) simulation

The SWISS-MODEL (https://swissmodel.expasy.org/) online tool was utilized to model the domains containing the mutated site, with the experimentally resolved structure (PDB: 6JFK) being the template [10]. Thereafter, MD analysis was conducted on the WT MFN2 and MFN2^{Ile213Thr} mutant models generated by Modeller9V17 [24]. Thereafter, this study utilized CHARMM22 program for the addition of C-/N-terminal patches and hydrogen atoms into models [25]. After solving and neutralizing the models generated within a box containing TIP3P water at least 13Å between box wall and the model, each simulation was run by NAMD 2.9 under the applied periodic boundary conditions (PBC) [26], with the pressure and temperature being kept at 1 atm and 300 K, respectively, using a time step of 2fs. In addition, electrostatics was modeled using particle mesh-Ewald approach, with the threshold of van der Waals force of 12Å. The two models were subjected to pre-equilibration at 3 steps with a total of 600 ps, and the final snapshots were selected to be the productive simulation starting structures (40 ns) with no constraints, respectively.

Results

Clinical manifestations

The pedigree diagram is exhibited in **Figure 1A**. As demonstrated by clinical examination, the proband exhibited typical CMT symptoms, including limb weakness, amyotrophy, clawed

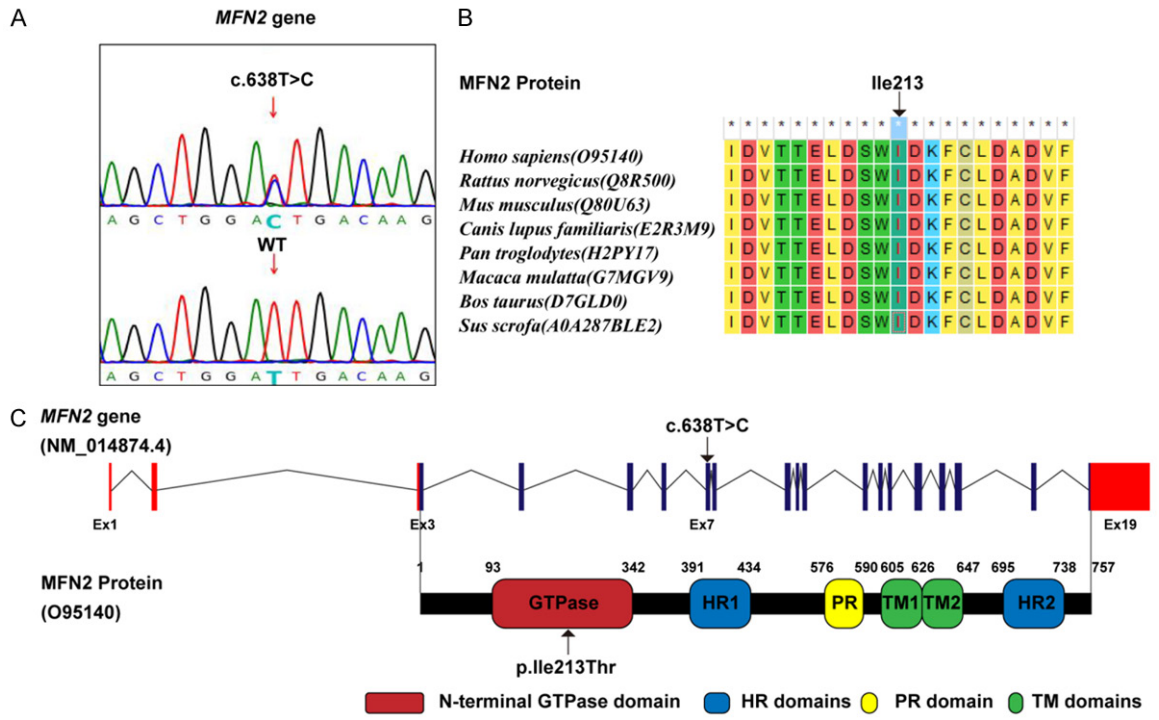

Figure 2. A. The identified variant *MFN2*: c. c.638T>C and wild-type (WT) control in Sanger sequencing peak diagrams. B. The evolutionary conservation of MFN2: Ile213 residue. C. The location of the c.638T>C (p.Ile213Thr) variant in the gene and protein schematic diagrams. HR, heptad repeat; PR, proline-rich; TM, transmembrane.

hands, strephenopodia, pes cavus, low limb muscle tension, and no tendon reflex (**Figure 1B**, **1C**). Results of electromyography (data shown in Supplementary Material 1) and peripheral nerve biopsy revealed serious demyelinating damage in peripheral nerves (**Figure 1D-F**). SEM detection showed the formation of numerous "onion bulbs" (**Figure 1G-I**).

The son of the proband has been displaying similar yet milder manifestations since the age of five.

Variation analysis of MFN2 gene

No CNV with clinical significance was observed according to the CMA results. WES identified a known pathogenic variant in MFN2 gene of the proband (II-2), which was NM_014874: c.638T>C (p.Ile213Thr) [27] (**Figure 2A**). Subsequent Sanger sequencing revealed that the son of the proband (III-1) also carried this variant, but prenatal diagnosis confirmed that the fetus (III-2) did not. The AA (Ile213) affected by this variant maintained evolutionarily conserved among species (**Figure 2B**). **Figure 2C** shows the location of the variant in the gene and protein schematic diagrams.

Metabolic profile affected by MFN2:p.Ile213Thr variation

According to the intracellular fluorescence signal of GFP (green fluorescent protein) internal control (containing the vector backbone) (**Figure 3A**) and the relative *MFN2* expression level (**Figure 3B**), all the vectors achieved ideal transfection efficiency.

Analysis results of metabolites with significant difference between the two groups (WT, Lab No. pHS-AVC-LY059; Mut, pHS-AVC-LY060) after transfection are demonstrated in **Figure 3C** and **3D**. Metabolic compounds with the most significant differences are listed in Supplementary Table 1 (the compound screening criteria were FC>2.0 or <0.5, P<0.05, vip >1. FC, fold count; vip, variable importance in projection). Pathway enrichment analysis indicated that the metabolic pathways most significantly affected by MFN2^{Ile213Thr} variant were the sphingolipid metabolism, glycerophospholipid metabolism, and flavin mononucleotide (FMN, one compound in the riboflavin) metabolism (**Figure 3E** and **Table 1**).

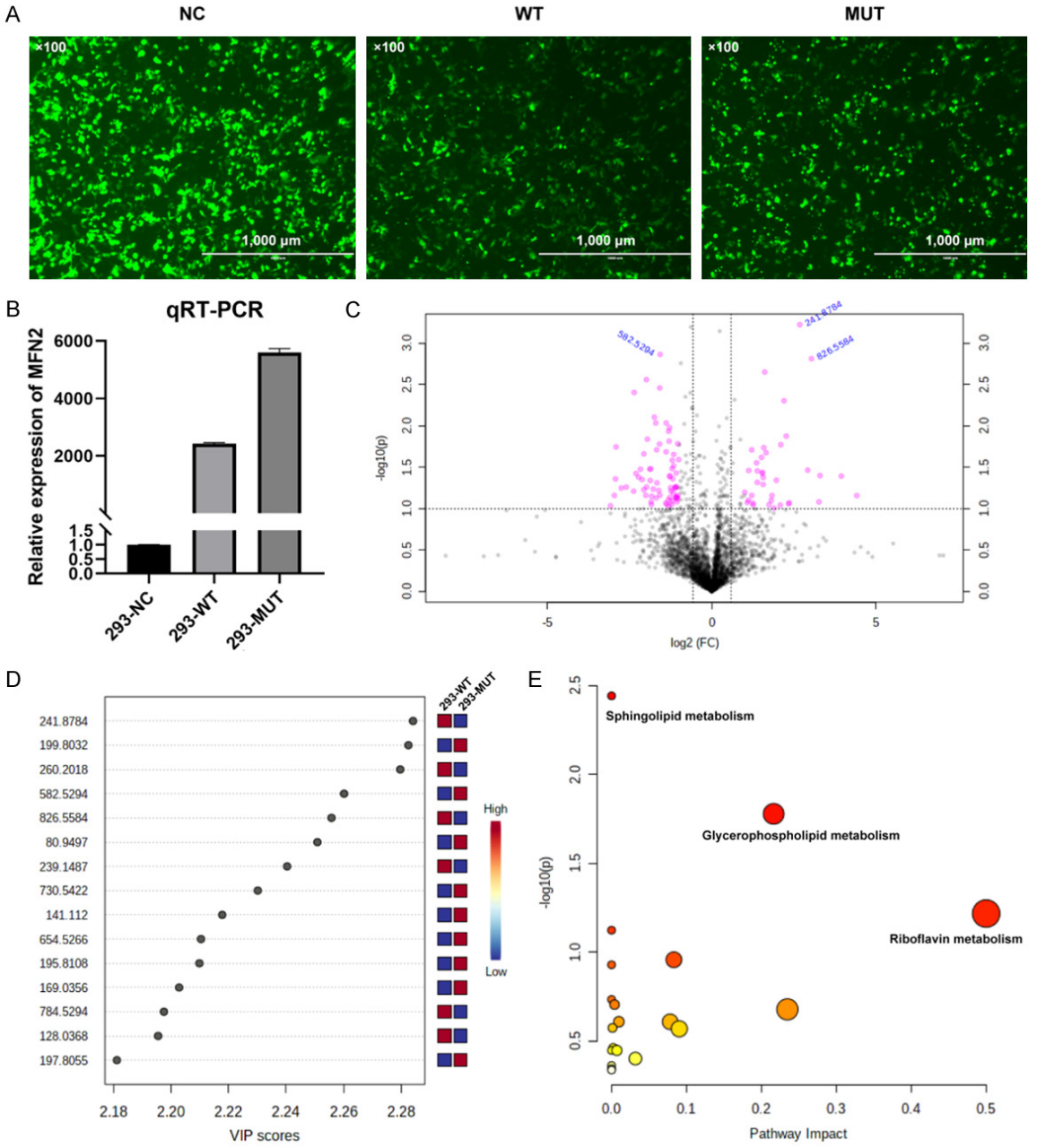

Figure 3. A. The GFP fluorescence signal at 48 h after transfection. NC, with plasmid backbone; WT, with wild-type *MFN2* cDNA; MUT, with *MFN2*: c.638T>C mutant cDNA. (Scale bar, 1000 μ; magnification: ×100). B. The relative MFN2 expression levels in 3 transfected cell groups. C. The volcano plot showing significantly different compounds. Red dots represent the difference >2.0 folds and P<0.05, blue font represents the m/z molecular weight information. D. Part of the compounds with vip (variable importance in projection) value >1. The X- and Y-axes stand for vip score and m/z, respectively. E. KEGG pathway enrichment result. Each point represents a pathway, with X- and Y-axes indicating the importance of a compound related to the pathway and-$\log_{10}$(P) value, respectively.

Intramolecular impact of MFN2: p.Ile213Thr variation

The overall and converged models of the WT and Ile213Thr mutant MFN2 are shown in **Figure 4A**, and the structures at different time points during MD are shown in **Figure 4B**. Clearly, the Ile213Thr model (abbreviated as I213T in this whole Figure) showed high flexibility compared with WT model based on root mean square fluctuation (RMSF) and root mean square deviation (RMSD) trajectory (**Figure 4C**

Table 1. Metabolic pathways most affected by MFN2: p.Ile213Thr variant (in reverse order of comprehensive significance)

KEGG (Kyoto Encyclopedia of Genes and Genomes)	Total	Hits	Raw P	Impact*
Sphingolipid metabolism	21	3	0.003616	0
Glycerophospholipid metabolism	36	3	0.016662	0.21631
Riboflavin metabolism	4	1	0.060569	0.5
Linoleic acid metabolism	5	1	0.075153	0
Amino sugar and nucleotide sugar metabolism	37	2	0.11021	0.08314
Ascorbate and aldarate metabolism	8	1	0.11761	0
alpha-Linolenic acid metabolism	13	1	0.18426	0
Glycosylphosphatidylinositol (GPI)-anchor biosynthesis	14	1	0.197	0.00399
Nicotinate and nicotinamide metabolism	15	1	0.20955	0.23465
Starch and sucrose metabolism	18	1	0.24607	0.00974
Pentose and glucuronate interconversions	18	1	0.24607	0.07812
Purine metabolism	65	2	0.2665	0.00124
Citrate cycle (TCA cycle)	20	1	0.26951	0.09038
Galactose metabolism	27	1	0.34619	0.00228
Alanine, aspartate and glutamate metabolism	28	1	0.35649	0
Glutathione metabolism	28	1	0.35649	0.00709
Glyoxylate and dicarboxylate metabolism	32	1	0.39617	0.03175
Arachidonic acid metabolism	36	1	0.4335	0
Arginine and proline metabolism	38	1	0.45132	0
Fatty acid degradation	39	1	0.46003	0

*, Total, overall compound number within a pathway; Hits, the number of data matched with those uploaded by the user; Raw P, raw *P*-value determined based on enrichment analysis; Impact, impact value of the pathway determined through pathway topological analysis.

and **4D**). Furthermore, Ile213Thr affected the interface residues in GTPase domain and the corresponding secondary structures (**Figure 4D-F**). Unsurprisingly, Ile213Thr formed more hydrogen bonds with the other residues than residue Ile213 (**Figure 4G**), but less with GTP than the WT model (**Figure 4H**), suggesting that the GTP binding ability became weaker in the mutant protein.

Discussion

Although CMT has been known for more than one hundred years, there are still some problems to be solved, such as better clinical differential diagnosis and better genotype-phenotype correlation, both of which should be achieved through further elucidating the structural and functional impacts of specific variations. The findings in the present study might provide a comprehensive perspective combining clinical, multi-omic, and *in silico* analyses to investigate the CMT causative variant.

The clinical and pathologic manifestations of the proband basically matched with the criteria of CMT, yet genetic investigation was still necessary to make a definite diagnosis. Subsequent analysis with WES identified a pathogenic variant, *MFN2*: c.638T>C: p.Ile213Thr, which was initially reported by Lawson *et al.* to cause CMT2A in the Caucasian population [27]. The son of the proband also carried this variant and presented kinetic symptoms since he was 5; fortunately, the fetus was not affected according to prenatal results. Low *et al.* revealed a progressively reduced density of myelinated fibers, and demyelination of more fibers, together with formation of more onion bulbs with age, as revealed by sural nerve biopsies of CMT patients [28]. This might explain the milder symptoms in the son despite the more severe clinical and pathologic indications in the proband. The identified variant was a missense variant located in the pivotal GTPase functional domain of MFN2, yet its particular impact was never fully clarified.

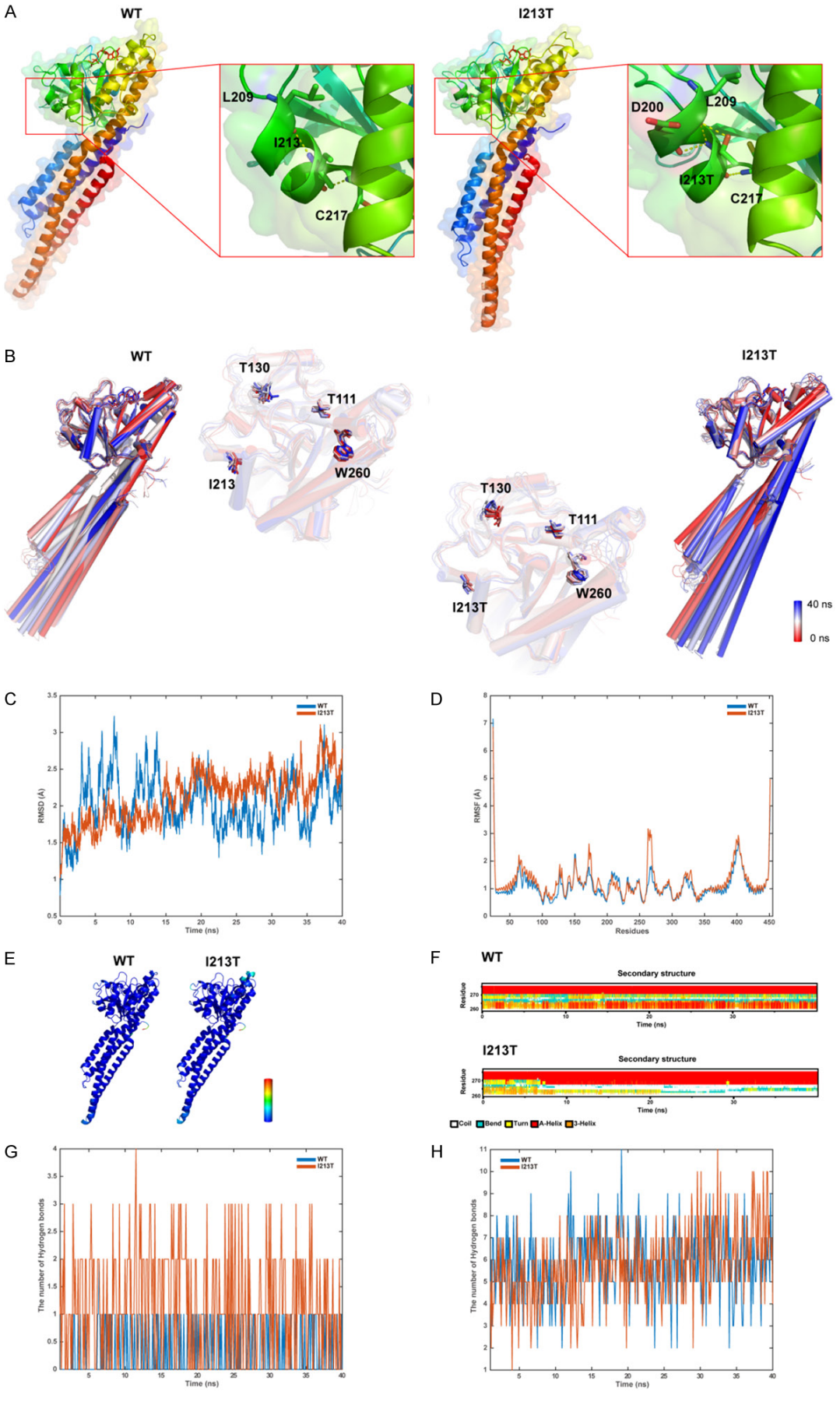
A
WT
L209
I213
C217
I213T
D200
L209
I213T
C217
B
WT
T130
T111
I213
W260
I213T
T130
T111
W260
I213T
40 ns
0 ns
C
RMSD (Å)
Time (ns)
WT
I213T
D
RMSF (Å)
Residues
WT
I213T
E
WT
I213T
F
WT
Secondary structure
Residue
Time (ns)
I213T
Secondary structure
Residue
Time (ns)
Coil
Bend
Turn
A-Helix
3-Helix
G
The number of hydrogen bonds
Time (ns)
WT
I213T
H
The number of hydrogen bonds
Time (ns)
WT
I213T

Figure 4. A. The structure models containing WT MFN2 and I213T mutant. Residues related to the formation of hydrogen bonds with residues I213 or I213T are represented by the sticks, and dotted yellow lines stand for hydrogen bonds. B. Superposition of 10 structural snapshots from 4 ns simulations of WT and I213T models. The backbone of the structures is shown as cartoon, with color from red to white to blue. C. The trajectory of RMSD (Cα) of the two proteins. D. RMSF for both proteins determined through every simulation. E. The WT/MUT models correlated according to RMSF. F. Secondary structural components in relevant area with time. G. Hydrogen bond formation between the residues I213 or I213T and the other residues, respectively. H. Hydrogen bond formation between I213 and GTP or I213T models, separately.

Mitofusins, including MFN1 and MFN2, regulate mitochondrial fusion, thus facilitating dynamic fusion-fission equilibrium determining mitochondrial morphology [29]. There are 1/3CMT2 patients with a family history who harbor the *MFN2* pathogenic variant [6]. Coiled-coiled and GTPase domain variations can result in early and severe disease onset, while C-terminal domain variations may induce mild and late disease onset [11, 30], yet the underlying mechanism remains unclear. In this study, we transfected the expression vectors containing WT or mutant (with p.Ile213Thr variant) MFN2 into cells *in vitro*, so as to detect differences in cell metabolite profiles. Pathway enrichment results demonstrated that this variant most probably affected phospholipid metabolism, especially for sphingolipids and glycerophospholipids. As shown in Supplementary Table 1, an important sphingolipid with significantly up-regulated expression was lysophosphatidylcholine (LysoPC), which was recognized to cause demyelination several decades ago [31]. Van Hameren *et al.* indicated that MFN2 defect and LysoPC-induced demyelination synergistically contributed to the reduction of ATP and elevation of reactive oxygen species (ROS), both of which were deleterious for neurons [32]. Another notably up-regulated sphingolipid was ceramide (with different modification, Supplementary Table 1). Parra *et al.* and Ausman *et al.* indicated that ceramide promoted mitochondrial fission and heightened cell autophagy [33, 34]. Additionally, another significantly down-regulated compound was FMN, the riboflavin kinase-generated metabolites. FMN has long been considered as an indispensable cofactor for the normal function of nitrite oxide synthase (NOS) and is involved in many cellular physiological processes including synaptic plasticity of nerves [35, 36]. Recently, it was recognized to act as a photosensitizer for m^6A RNA demethylation, indicating a necessity to further explore its biologic functions and application value in disease therapy [37]. However, only preliminary metabonomic results were obtained by this study. The underlying mechanism by which MFN2 variation affects small molecules metabolism and how this effect induces CMT manifestation still need further investigation [38].

MFN2, the GTPase located on the outer mitochondrial membrane, regulates the fusion and fission of mitochondria [11]. GTPase activity is required for the normal MFN2 function. In this regard, in MD simulation analysis, we chose the experimentally resolved structure with GTP (PDB: 6JFK) as the template [10] to build the models with attached GTP. The affected AA residue, Ile213, belongs to the GTPase domain and is close to the catalytic site. According to the result, the p.Ile213Thr variant, which replaced the extremely hydrophobic residue by a polar amino acid, expectantly formed hydrogen bonds by the side chain of Thr213 to change the surrounding conformation. This might significantly perturb the MFN2 homodimerization via the GTPase(G) interface, whereas MFN2 should form the persistent dimers following GTP hydrolysis through G interface [10]. In the protein structure, it is recognized that Thr111 is the phosphorylation site, while Thr130 is the catalytic site, and the side chain of Trp260 can occupy the nucleotide-binding pocket [10]. According to MD results, the motion amplitude of these key and catalytic residues increased because of this variant, which might affect binding to GTP. These findings generally supported the reduced ability of MFN2 to bind to GTP by this variation. However, functional experiments are still needed to validate these simulations.

Rocha *et al.* adopted a small molecular MFN2 agonist to normalize sciatic nerve axonal mitochondrial trafficking in mice with Mfn2 mutant [39], while Zeng *et al.* also proved that the small molecular echinacoside improved mitochondrial fusion [40], both of which provided a good prospect for the future treatment of CMT2A. But more investigations are needed to illustrate the function and structure of mutant MFN2 for

the development of small molecule-based treatment strategies.

Certain limitations should be noted in this study. First of all, there were no deep functional experimental results to demonstrate our findings. For this, we will design complete *in vitro* and *in vivo* experimental models in combination with complete molecular biology validation to clarify the underlying pathogenic mechanism.

Conclusions

In summary, we recruited an autosomal dominant CMT case and detected the causative pathogenic variant *MFN2*: c.638T>C: p.Ile213Thr. *In vitro* study indicated that this variant might affect cell metabolism in phospholipids. MD simulation suggested that this variant might damage the binding ability of MFN2 to GTP. Nonetheless, further functional and mechanistic studies are needed to prove these findings. This study may shed new light on the impact of specific MFN2 variants.

Acknowledgements

Our thanks go to the participants for taking part in this study.

Disclosure of conflict of interest

None.

Address correspondence to: Cheng-Hong Yin, Prenatal Diagnosis Center, Beijing Obstetrics and Gynecology Hospital, Capital Medical University, 251 Yaojiayuan Road, Beijing 100083, China. Tel: +86-010-52275426; E-mail: yinchh@ccmu.edu.cn; Qing Guo, Prenatal Diagnosis Center, Shijiazhuang Obstetrics and Gynecology Hospital, 206 East Zhongshan Road, Shijiazhuang 050011, Hebei, China. E-mail: yfguoqing@163.com

References

[1] Nagappa M, Sharma S and Taly AB. Charcot Marie Tooth. Treasure Island (FL): StatPearls Publishing; 2020.

[2] Laurá M, Singh D, Ramdharry G, Morrow J, Skorupinska M, Pareyson D, Burns J, Lewis RA, Scherer SS, Herrmann DN, Cullen N, Bradish C, Gaiani L, Martinelli N, Gibbons P, Pfeffer G, Phisitkul P, Wapner K, Sanders J, Flemister S, Shy ME and Reilly MM; Inherited Neuropathies Consortium. CMT subtypes and disease burden in patients enrolled in the Inherited Neuropathies Consortium natural history study: a cross-sectional analysis. J Neurol Neurosurg Psychiatry 2015; 86: 873-878.

[3] Laura M, Pipis M, Rossor AM and Reilly MM. Charcot-Marie-Tooth disease and related disorders: an evolving landscape. Curr Opin Neurol 2019; 32: 641-650.

[4] Bergamin G, Boaretto F, Briani C, Pegoraro E, Cacciavillani M, Martinuzzi A, Muglia M, Vettori A, Vazza G and Mostacciuolo ML. Mutation analysis of MFN2, GJB1, MPZ and PMP22 in Italian patients with axonal charcot-marie-tooth disease. Neuromol Med 2014; 16: 540-550.

[5] Züchner S. MFN2 Hereditary Motor and Sensory Neuropathy. In: Adam MP, Ardinger HH, Pagon RA, Wallace SE, Bean LJH, Mirzaa G, Amemiya A, editors. Seattle (WA), University of Washington: Seattle; 2020.

[6] Verhoeven K, Claeys KG, Zuchner S, Schroder JM, Weis J, Ceuterick C, Jordanova A, Nelis E, De Vriendt E, Van Hul M, Seeman P, Mazanec R, Saifi GM, Szigeti K, Mancias P, Butler IJ, Kochanski A, Ryniewicz B, De Bleecker J, Van den Bergh P, Verellen C, Van Coster R, Goemans N, Auer-Grumbach M, Robberecht W, Milic Rasic V, Nevo Y, Tournev I, Guergueltcheva V, Roelens F, Vieregge P, Vinci P, Moreno MT, Christen HJ, Shy ME, Lupski JR, Vance JM, De Jonghe P and Timmerman V. MFN2 mutation distribution and genotype/phenotype correlation in Charcot-Marie-Tooth type 2. Brain 2006; 129: 2093-2102.

[7] Züchner S, Mersiyanova IV, Muglia M, Bissar-Tadmouri N, Rochelle J, Dadali EL, Zappia M, Nelis E, Patitucci A, Senderek J, Parman Y, Evgrafov O, Jonghe PD, Takahashi Y, Tsuji S, Pericak-Vance MA, Quattrone A, Battaloglu E, Polyakov AV, Timmerman V, Schroder JM and Vance JM. Mutations in the mitochondrial GTPase mitofusin 2 cause Charcot-Marie-Tooth neuropathy type 2A. Nat Genet 2004; 36: 449-451.

[8] Yoshimura A, Yuan JH, Hashiguchi A, Ando M, Higuchi Y, Nakamura T, Okamoto Y, Nakagawa M and Takashima H. Genetic profile and onset features of 1005 patients with Charcot-Marie-Tooth disease in Japan. J Neurol Neurosurg Psychiatry 2019; 90: 195-202.

[9] Padilha JPD, Brasil CS, Hoefel AML, Winckler PB, Donis KC, Brusius-Facchin AC and Saute JAM. Diagnostic yield of targeted sequential and massive panel approaches for inherited neuropathies. Clin Genet 2020; 98: 185-190.

[10] Li YJ, Cao YL, Feng JX, Qi Y, Meng S, Yang JF, Zhong YT, Kang S, Chen X, Lan L, Luo L, Yu B, Chen S, Chan DC, Hu J and Gao S. Structural

insights of human mitofusin-2 into mitochondrial fusion and CMT2A onset. Nat Commun 2019; 10: 4914.
[11] Dorn GW 2nd. Mitofusin 2 dysfunction and disease in mice and men. Front Physiol 2020; 11: 782.
[12] Filadi R, Pendin D and Pizzo P. Mitofusin 2: from functions to disease. Cell Death Dis 2018; 9: 330.
[13] Leal NS, Schreiner B, Pinho CM, Filadi R, Wiehager B, Karlstrom H, Pizzo P and Ankarcrona M. Mitofusin-2 knockdown increases ER-mitochondria contact and decreases amyloid beta-peptide production. J Cell Mol Med 2016; 20: 1686-1695.
[14] Chen H, Detmer SA, Ewald AJ, Griffin EE, Fraser SE and Chan DC. Mitofusins Mfn1 and Mfn2 coordinately regulate mitochondrial fusion and are essential for embryonic development. J Cell Biol 2003; 160: 189-200.
[15] Chen H, McCaffery JM and Chan DC. Mitochondrial fusion protects against neurodegeneration in the cerebellum. Cell 2007; 130: 548-562.
[16] Bach D, Naon D, Pich S, Soriano FX, Vega N, Rieusset J and Laville M. Expression of Mfn2, the Charcot-Marie-Tooth neuropathy type 2A gene, in human skeletal muscle: effects of type 2 diabetes, obesity, weight loss, and the regulatory role of tumor necrosis factor α and interleukin-6. Diabetes 2005; 54: 2685-2693.
[17] Xu L, Wu Z, He Y, Chen Z, Xu K, Yu W, Fang W, Ma C, Moqbel SAA, Ran J, Xiong Y and Wu L. MFN2 contributes to metabolic disorders and inflammation in the aging of rat chondrocytes and osteoarthritis. Osteoarthritis Cartilage 2020; 28: 1079-1091.
[18] Franco A, Kitsis RN, Fleischer JA, Gavathiotis E, Kornfeld OS, Gong G, Biris N, Benz A, Qvit N, Donnelly SK, Chen Y, Mennerick S, Hodgson L, Mochly-Rosen D and Dorn GW II. Correcting mitochondrial fusion by manipulating mitofusin conformations. Nature 2016; 540: 74-79.
[19] Dang X, Zhang L, Franco A, Li J, Rocha AG, Devanathan S, Dolle RE, Bernstein PR and Dorn GW 2nd. Discovery of 6-phenylhexanamide derivatives as potent stereoselective mitofusin activators for the treatment of mitochondrial diseases. J Med Chem 2020; 63: 7033-7051.
[20] Samanas NB, Engelhart EA and Hoppins S. Defective nucleotide-dependent assembly and membrane fusion in Mfn2 CMT2A variants improved by Bax. Life Sci Alliance 2020; 3: e201900527.
[21] Yang K, Shen M, Yan Y, Tan Y, Zhang J, Wu J, Yang G, Li S, Wang J, Ren Z, Dong Z, Wang S, Zhang M and Tian Y. Genetic analysis in fetal skeletal dysplasias by trio whole-exome sequencing. Biomed Res Int 2019; 2019: 2492590.
[22] Wang K, Li M and Hakonarson H. ANNOVAR: functional annotation of genetic variants from next-generation sequencing data. Nucleic Acids Research 2010; 38: e164.
[23] Richards S, Aziz N, Bale S, Bick D, Das S, Gastier-Foster J, Grody WW, Hegde M, Lyon E, Spector E, Voelkerding K and Rehm HL; ACMG Laboratory Quality Assurance Committee. Standards and guidelines for the interpretation of sequence variants: a joint consensus recommendation of the American college of medical genetics and genomics and the association for molecular pathology. Genet Med 2015; 17: 405-424.
[24] Webb B and Sali A. Comparative protein structure modeling using MODELLER. Curr Protoc Bioinformatics 2016; 54: 5.6.1-5.6.37.
[25] MacKerell AD, Bashford D, Bellott M, Dunbrack RL, Evanseck JD, Field MJ, Fischer S, Gao J, Guo H and Ha S. All-atom empirical potential for molecular modeling and dynamics studies of proteins. J Phys Chem B 1998; 102: 3586-3616.
[26] Phillips JC, Hardy DJ, Maia JDC, Stone JE, Ribeiro JV, Bernardi RC, Buch R, Fiorin G, Henin J, Jiang W, McGreevy R, Melo MCR, Radak BK, Skeel RD, Singharoy A, Wang Y, Roux B, Aksimentiev A, Luthey-Schulten Z, Kale LV, Schulten K, Chipot C and Tajkhorshid E. Scalable molecular dynamics on CPU and GPU architectures with NAMD. J Chem Phys 2020; 153: 044130.
[27] Lawson VH, Brad V. Graham B and Flanigan KM. Clinical and electrophysiologic features of CMT2A with mutations in the mitofusin 2 gene. Neurology 2005; 65: 197-204.
[28] Low PA, McLeod JG and Prineas JW. Hypertrophic Charcot-Marie-Tooth disease: light and electron microscope studies of the sural nerve. J Neurol Sci 1978; 35: 93-115.
[29] Santel A and Fuller MT. Control of mitochondrial morphology by a human mitofusin. J Cell Sci 2001; 114: 867-874.
[30] Feely SME, Laura M, Siskind CE, Sottile S, Davis M, Gibbons VS, Reilly MM and Shy ME. MFN2 mutations cause severe phenotypes in most patients with CMT2A. Neurology 2011; 76: 1690-1696.
[31] Plemel JR, Michaels NJ, Weishaupt N, Caprariello AV, Keough MB, Rogers JA, Yukseloglu A, Lim J, Patel VV, Rawji KS, Jensen SK, Teo W, Heyne B, Whitehead SN, Stys PK and Yong VW. Mechanisms of lysophosphatidylcholine-induced demyelination: a primary lipid disrupting myelinopathy. Glia 2018; 66: 327-347.
[32] van Hameren G, Campbell G, Deck M, Berthelot J, Gautier B, Quintana P, Chrast R and Tricaud

N. In vivo real-time dynamics of ATP and ROS production in axonal mitochondria show decoupling in mouse models of peripheral neuropathies. Acta Neuropathol Commun 2019; 7: 86.

[33] Ausman J, Abbade J, Ermini L, Farrell A, Tagliaferro A, Post M and Caniggia I. Ceramide-induced BOK promotes mitochondrial fission in preeclampsia. Cell Death Dis 2018; 9: 298.

[34] Parra V, Eisner V, Chiong M, Criollo A, Moraga F, Garcia A, Hartel S, Jaimovich E, Zorzano A, Hidalgo C and Lavandero S. Changes in mitochondrial dynamics during ceramide-induced cardiomyocyte early apoptosis. Cardiovasc Res 2008; 77: 387-397.

[35] Liu XD, Mazumdar T, Xu Y, Getzoff ED and Eissa NT. Identification of a flavin mononucleotide module residue critical for activity of inducible nitrite oxide synthase. J Immunol 2009; 183: 5977-5982.

[36] Forstermann U and Sessa WC. Nitric oxide synthases: regulation and function. Eur Heart J 2011; 33: 829-37, 837a-837d.

[37] Xie LJ, Yang XT, Wang RL, Cheng HP, Li ZY, Liu L, Mao L, Wang M and Cheng L. Identification of flavin mononucleotide as a cell-active artificial N6emethyladenosine RNA demethylase. Angew Chem Int Ed Engl 2019; 58: 5028-5032.

[38] Fugio LB, Coeli-Lacchini FB and Leopoldino AM. Sphingolipids and mitochondrial dynamic. Cells 2020; 9: 581.

[39] Rocha AG, Franco A, Krezel AM, Rumsey JM, Alberti JM, Knight WC, Biris N, Zacharioudakis E, Janetka JW, Baloh RH, Kitsis RN, Mochly-Rosen D, Townsend RR, Gavathiotis E and Dorn GW 2nd. MFN2 agonists reverse mitochondrial defects in preclinical models of Charcot-Marie-Tooth disease type 2A. Science 2018; 360: 336-341.

[40] Zeng KW, Wang JK, Wang LC, Guo Q, Liu TT, Wang FJ, Feng N, Zhang XW, Liao LX, Zhao MM, Liu D, Jiang Y and Tu P. Small molecule induces mitochondrial fusion for neuroprotection via targeting CK2 without affecting its conventional kinase activity. Signal Transduct Target Ther 2021; 6: 71.

Supplementary Material 1

1. Electromyography results of the proband.

Muscles	Side	Slack status					With mild force					With heavy force					Other
		Inserted potential	fibrillation potential	positive potential	Myotonic potential	Beam fibrillation potential	average time (ms)	average amplitude (mv)	polyphasic potential	giant potential	Myopathy potential	Interference phase	mixed phase	pure phase	largest amplitude	pathological interference phase	
tibialis anterior	left	10	10	10			↑	↑						√			
peroneus longus	left	10	10	10			↑	↑						√			
extensor digitorum brevis	left	10	10	20			↑	↑						√			
musculus gastrocnemius	left	0					0	0						√			
medial vastus muscle	left	0					↑	↑						√			
tibialis anterior	right	10	10	20			↑	↑						√			
peroneus longus	right	10	10	10			↑	↑						√			
extensor digitorum brevis	right	10	10	20			↑	↑						√			
musculus gastrocnemius	right	0					0↑	0↑						√			
medial vastus muscle	right	10	10	10			↑	↑						√			
paravertebral muscle T11	right	-		10			↑	↑									
paravertebral muscle T12	left	0					0	0									
first dorsal interosseus	left	0					↑	↑						√			
musculi abductor pollicis brevis	left	0					↑	↑					√	√			
extensor digitorum	left	0					↑	↑					√				
deltoideus triangularis	left	0					0	0					√				
bicipital muscle of arm	left	0					0	0					√				
first dorsal interosseus	right	-	±	±			↑	↑						√			
musculi abductor pollicis brevis	right	0					0↑	0↑					√				
extensor digitorum	right	0					0	0					√				
deltoideus triangularis	right	0					0	0					√				
bicipital muscle of arm	right	0					0	0					√				

Motor nerve conduction								
Nerve	Stimulating spot	Recording spot	Latency time (ms)		Amplitude (mv)		Conduction velocity or excitation rate (m/s)		Other
			left	right	left	right	left	right	
deep peroneal nerve	Capitula fibula	tibialis anterior	12.2	20.1	8.4	4.6	11	7	
superficial peroneal nerve	Capitula fibula	peroneus longus	14.4	13.8	5.6	7.4	9	11	
total peroneal nerve	ankle	extensor digitorum brevis	25.8	7.2	2.8	2.7	7	12	
	Capitula fibula		87.0	32.9	2.5	2.7			
nervus tibialis	popliteal fossa	musculus gastrocnemius	16.0	30.3	8.6	3.2	10	7	
nervus femoralis		medial vastus muscle	39.4	71.8	2.3	1.0	7	3	
ulnar nerve	wrist	first dorsal interosseus	15.1	10.9	7.9	11.4	5	6	Waveform from several
	elbow		59.8	53.2	9.0	6.4			Waveform from several
nervus medianus	wrist	musculi abductor pollicis brevis	11.8	12.0	3.8	2.3	4	5	Waveform from several
	elbow		58.5	54.6	4.1	1.4			Waveform from several
musculospiralis	radial groove	extensor digitorum	28.9	28.1	2.9	2.3	7	8	Waveform from several
musculocutaneous nerve	ERB'S	deltoideus triangularis	28.7	20.6	2.0	2.9	9	11	Waveform from several
axillary nerve	ERB'S	bicipital muscle of arm	12.1	26.2	6.1	6.7	12	6	Waveform from several
Sensory nerve conduction									
Nerve	Stimulating spot	Recording spot	Latency time (ms)		Amplitude (mv)		Excitation rate (m/s)		Other
			left	right	left	right	left	right	
ulnar nerve	little finger	wrist	no SNAP	no SNAP					
nervus medianus	digitus medius	wrist	no SNAP	no SNAP					
superficial peroneal nerve			no SNAP	no SNAP					
nervus suralis			no SNAP	no SNAP					

Results description: Electromyography shows fibrillar, positive phase potential, action potential amplitude, time-limit widening increased when light force; Motor nerve conduction amplitude is normal/mild decrease; nerve conduction velocity is about 10 m/s (which is unusual in CMT2A); sensory nerve conduction is seriously without SNAP.

2. Detailed data of the vector construction and cell transfection.

(1) cDNA sequences

No. pHS-AVC-LY059 (wild-type) MFN2 (human, NM_014874)

5'-ATGTCCCTGCTCTTCTCTCGATGCAACTCTATCGTCACAGTCAAGAAAAATAAGAGACACATGGCTGAGGTG-
AATGCATCCCCACTTAAGCACTTTGTCACTGCCAAGAAGAAGATCAATGGCATTTTTGAGCAGCTGGGGGCCTAC-
ATCCAGGAGAGCGCCACCTTCCTTGAAGACACGTACAGGAATGCAGAACTGGACCCCGTTACCACAGAAGAACA-
GGTTCTGGACGTCAAAGGTTACCTATCCAAAGTGAGAGGCATCAGTGAGGTGCTGGCTCGGAGGCACATG-
AAAGTGGCTTTTTTTGGCCGGACGAGCAATGGGAAGAGCACCGTGATCAATGCCATGCTCTGGGACAAAGTTCT-
GCCCTCTGGGATTGGCCACACCACCAATTGCTTCCTGCGGGTAGAGGGCACAGATGGCCATGAGGCCTTTCTCC-
TTACCGAGGGCTCAGAGGAAAAGAGGAGTGCCAAGACTGTGAACCAGCTGGCCCATGCCCTCCACCAGGACAA-
GCAGCTCCATGCCGGCAGCCTAGTGAGTGTGATGTGGCCCAACTCTAAGTGCCCACTTCTGAAGGATGACCTCG-
TTTTGATGGACAGCCCTGGTATTGATGTCACCACAGAGCTGGACAGCTGGATTGACAAGTTTTGTCTGGATGCT-
GATGTGTTTGTGCTGGTGGCCAACTCAGAGTCCACCCTGATGCAGACGGAAAAGCACTTCTTCCACAAGGTGA-
GTGAGCGTCTCTCCCGGCCAAACATCTTCATCCTGAACAACCGCTGGGATGCATCTGCCTCAGAGCCCGAGTAC-
ATGGAGGAGGTGCGGCGGCAGCACATGGAGCGTTGTACCAGCTTCCTGGTGGATGAGCTGGGCGTGGTGGATC-
GATCCCAGGCCGGGGACCGCATCTTCTTTGTGTCTGCTAAGGAGGTGCTCAACGCCAGGATTCAGAAAGCCCA-
GGGCATGCCTGAAGGAGGGGGCGCTCTCGCAGAAGGCTTTCAAGTGAGGATGTTTGAGTTTCAGAATTTTGAG-
AGGAGATTTGAGGAGTGCATCTCCCAGTCTGCAGTGAAGACCAAGTTTGAGCAGCACACGGTCCGGGCCAAGC-
AGATTGCAGAGGCGGTTCGACTCATCATGGACTCCCTGCACATGGCGGCTCGGGAGCAGCAGGTTTACTGCGA-
GGAAATGCGTGAAGAGCGGCAAGACCGACTGAAATTTATTGACAAACAGCTGGAGCTCTTGGCTCAAGACTA-
TAAGCTGCGAATTAAGCAGATTACGGAGGAAGTGGAGAGGCAGGTGTCGACTGCAATGGCCGAGGAGATC-
AGGCGCCTCTCTGTACTGGTGGACGATTACCAGATGGACTTCCACCCTTCTCCAGTAGTCCTCAAGGTTTATAA-
GAATGAGCTGCACCGCCACATAGAGGAAGGACTGGGTCGAAACATGTCTGACCGCTGCTCCACGGCCATCAC-
CAACTCCCTGCAGACCATGCAGCAGGACATGATAGATGGCTTGAAACCCCTCCTTCCTGTGTCTGTGCGGAG-
TCAGATAGACATGCTGGTCCCACGCCAGTGCTTCTCCCTCAACTATGACCTAAACTGTGACAAGCTGTGTGCT-
GACTTCCAGGAAGACATTGAGTTCCATTTCTCTCTCGGATGGACCATGCTGGTGAATAGGTTCCTGGGCCCCA-
AGAACAGCCGTCGGGCCTTGATGGGCTACAATGACCAGGTCCAGCGTCCCATCCCTCTGACGCCAGCCAACCC-
CAGCATGCCCCCACTGCCACAGGGCTCGCTCACCCAGGAGGAGTTCATGGTTTCCATGGTTACCGGCCTGGCC-
TCCTTGACATCCAGGACCTCCATGGGCATTCTTGTTGTTGGAGGAGTGGTGTGGAAGGCAGTGGGCTGGCGG-
CTCATTGCCCTCTCCTTTGGGCTCTATGGCCTCCTCTACGTCTATGAGCGTCTGACCTGGACCACCAAGGCCAA-
GGAGAGGGCCTTCAAGCGCCAGTTTGTGGAGCATGCCAGCGAGAAGCTGCAGCTTGTCATCAGCTACACTGG-
CTCCAACTGCAGCCACCAAGTCCAGCAGGAACTGTCTGGGACCTTTGCTCATCTGTGTCAGCAAGTTGACGTC-
ACCCGGGAGAACCTGGAGCAGGAAATTGCCGCCATGAACAAGAAAATTGAGGTTCTTGACTCACTTCAGAGCA-
AAGCAAAGCTGCTCAGGAATAAAGCCGGTTGGTTGGACAGTGAGCTCAACATGTTCACACACCAGTACCTGCA-
GCCCAGCAGA-3'

No. pHS-AVC-LY060 (mutant) MFN2(human,NM_014874, 638T>C)

5'-ATGTCCCTGCTCTTCTCTCGATGCAACTCTATCGTCACAGTCAAGAAAAATAAGAGACACATGGCTGAGGT-
GAATGCATCCCCACTTAAGCACTTTGTCACTGCCAAGAAGAAGATCAATGGCATTTTTGAGCAGCTGGGGGCC-
TACATCCAGGAGAGCGCCACCTTCCTTGAAGACACGTACAGGAATGCAGAACTGGACCCCGTTACCACAGAAG-
AACAGGTTCTGGACGTCAAAGGTTACCTATCCAAAGTGAGAGGCATCAGTGAGGTGCTGGCTCGGAGGCACAT-
GAAAGTGGCTTTTTTTGGCCGGACGAGCAATGGGAAGAGCACCGTGATCAATGCCATGCTCTGGGACAAAGTT-
CTGCCCTCTGGGATTGGCCACACCACCAATTGCTTCCTGCGGGTAGAGGGCACAGATGGCCATGAGGCCTTTC-
TCCTTACCGAGGGCTCAGAGGAAAAGAGGAGTGCCAAGACTGTGAACCAGCTGGCCCATGCCCTCCACCAGG-
ACAAGCAGCTCCATGCCGGCAGCCTAGTGAGTGTGATGTGGCCCAACTCTAAGTGCCCACTTCTGAAGGATG-
ACCTCGTTTTGATGGACAGCCCTGGTATTGATGTCACCACAGAGCTGGACAGCTGGACTGACAAGTTTTGTCT-
GGATGCTGATGTGTTTGTGCTGGTGGCCAACTCAGAGTCCACCCTGATGCAGACGGAAAAGCACTTCTTCCA-
CAAGGTGAGTGAGCGTCTCTCCCGGCCAAACATCTTCATCCTGAACAACCGCTGGGATGCATCTGCCTCAGA-
GCCCGAGTACATGGAGGAGGTGCGGCGGCAGCACATGGAGCGTTGTACCAGCTTCCTGGTGGATGAGCTGGG-
CGTGGTGGATCGATCCCAGGCCGGGGACCGCATCTTCTTTGTGTCTGCTAAGGAGGTGCTCAACGCCAGGATT-
CAGAAAGCCCAGGGCATGCCTGAAGGAGGGGGCGCTCTCGCAGAAGGCTTTCAAGTGAGGATGTTTGAGTT-
TCAGAATTTTGAGAGGAGATTTGAGGAGTGCATCTCCCAGTCTGCAGTGAAGACCAAGTTTGAGCAGCACACG-
GTCCGGGCCAAGCAGATTGCAGAGGCGGTTCGACTCATCATGGACTCCCTGCACATGGCGGCTCGGGAGCAG-

CAGGTTTACTGCGAGGAAATGCGTGAAGAGCGGCAAGACCGACTGAAATTTATTGACAAACAGCTGGAGCTCT-TGGCTCAAGACTATAAGCTGCGAATTAAGCAGATTACGGAGGAAGTGGAGAGGCAGGTGTCGACTGCAATGG-CCGAGGAGATCAGGCGCCTCTCTGTACTGGTGGACGATTACCAGATGGACTTCCACCCTTCTCCAGTAGTCC-TCAAGGTTTATAAGAATGAGCTGCACCGCCACATAGAGGAAGGACTGGGTCGAAACATGTCTGACCGCTGC-TCCACGGCCATCACCAACTCCCTGCAGACCATGCAGCAGGACATGATAGATGGCTTGAAACCCCTCCTTCCT-GTGTCTGTGCGGAGTCAGATAGACATGCTGGTCCCACGCCAGTGCTTCTCCCTCAACTATGACCTAAACTGT-GACAAGCTGTGTGCTGACTTCCAGGAAGACATTGAGTTCCATTTCTCTCTCGGATGGACCATGCTGGTGAATA-GGTTCCTGGGCCCCAAGAACAGCCGTCGGGCCTTGATGGGCTACAATGACCAGGTCCAGCGTCCCATCCCTC-TGACGCCAGCCAACCCCAGCATGCCCCCACTGCCACAGGGCTCGCTCACCCAGGAGGAGTTCATGGTTTCC-ATGGTTACCGGCCTGGCCTCCTTGACATCCAGGACCTCCATGGGCATTCTTGTTGTTGGAGGAGTGGTGTGG-AAGGCAGTGGGCTGGCGGCTCATTGCCCTCTCCTTTGGGCTCTATGGCCTCCTCTACGTCTATGAGCGTCTGA-CCTGGACCACCAAGGCCAAGGAGAGGGCCTTCAAGCGCCAGTTTGTGGAGCATGCCAGCGAGAAGCTGCAG-CTTGTCATCAGCTACACTGGCTCCAACTGCAGCCACCAAGTCCAGCAGGAACTGTCTGGGACCTTTGCTCATC-TGTGTCAGCAAGTTGACGTCACCCGGGAGAACCTGGAGCAGGAAATTGCCGCCATGAACAAGAAAATTGAG-GTTCTTGACTCACTTCAGAGCAAAGCAAAGCTGCTCAGGAATAAAGCCGGTTGGTTGGACAGTGAGCTCAACA-TGTTCACACACCAGTACCTGCAGCCCAGCAGA-3'

(2) Vector backbone diagram

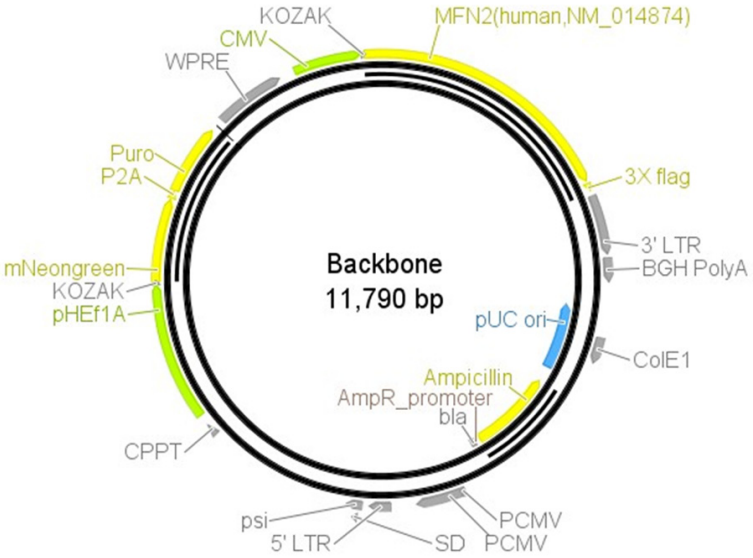

(3) Primers used in the vector construction and QF-PCR

Target	Forward-primer	Reverse-primer	Segment length (bp)
MFN2	GGACCCCGTTACCACAGAAG	TTGTCCCAGAGCATGGCATT	162
MFN2 (638T>C)	GGACCCCGTTACCACAGAAG	TTGTCCCAGAGCATGGCATT	162
GAPDH	TGACTTCAACAGCGACACCCA	CACCCTGTTGCTGTAGCCAAA	121

(4) Data of QF-PCR (48 h after transfection)

Gene	Group	Repetition 1	Repetition 2	Repetition 3	Mean	SD	QC[1]
MFN2	293FT	0.3	0.3	0.3	0.315	0.014	0.046
	293FT-pHS-AVC-LY059	2452.4	2435.5	2385.4	2424.436	34.872	0.014
	293FT-pHS-AVC-LY060	5673.4	5673.4	5442.3	5596.371	133.432	0.024
	293FT-pHS-BVC-LW345	1.0	1.0	1.0	1.000	0.012	0.012

[1]QC, the value of standard deviation/mean. The larger the value, the higher the volatility of the experimental data.

Supplementary Table 1. List of differentiated compounds

m/z	FC (pHS-AVC-LY059/ pHS-AVC-LY060)	log2(FC)	raw. pval	vip	compound_id	compound_ name	adduct	delta (ppm)	sub-class	Source	KEGG_ com-pound	KEGG_ pathway	KEGG_pathway_descriptionn
89.9414	3.5093	1.8112	0.079369	1.7718	HMDB0013667	Yttrium	[M+H]+	315	-	Endog-enous	-	-	-
116.9269	3.9056	1.9656	0.045241	1.9133	HMDB0029596	Chloroform	[M-H]-	169	Halo-meth-anes	Endog-enous|Food|Environ-mental|Biological	C13827	-	-
122.0958	0.46894	-1.0925	0.072381	1.798	HMDB0001020	N, N-Dimethyl-aniline	[M+H]+	5	Amines	Endog-enous|Food|Biological	C02846	-	-
128.0368	4.5875	2.1977	0.004952	2.1955	HMDB0000267	L-5-Oxoproline	[M-H]-	12	Amino acids, peptides, and ana-logues	Endog-enous|Food|Biological	C01879	map00480; map01100	Glutathione metabolism; Metabolic pathways
137.0271	0.46029	-1.1194	0.055543	1.8665	HMDB0000500	4-Hydroxyben-zoic acid	[M-H]-	20	Benzoic acids and deriva-tives	Endog-enous|Food|Biological	C00156	map00130; map00362; map00363; map00623; map00627; map00790; map01061; map01100; map01110; map01120; map01220; map01240; map07110	Ubiquinone and other terpenoid-quinone bio-synthesis; Benzoate degradation; Bisphenol degradation; Toluene degradation; Amino-benzoate degradation; Folate biosynthesis; Biosynthesis of phenylpropanoids; Metabolic pathways; Biosynthesis of secondary metabo-lites; Microbial metabolism in diverse environ-ments; Degradation of aromatic compounds; Biosynthesis of cofactors; Benzoic acid family
141.112	0.33401	-1.582	0.003465	2.2178	HMDB0029598	Metenamine	[M+H]+	11	1,3,5-tri-azinanes	Endog-enous|Food	-	-	-
167.0225	0.46796	-1.0955	0.054323	1.8719	HMDB0000289	Uric acid	[M-H]-	9	Purines and purine deriva-tives	Endog-enous|Food|Biological	C00366	map00230; map01100; map01120; map04976	Purine metabolism; Metabolic pathways; Mi-crobial metabolism in diverse environments; Bile secretion

191.0215	9.5827	3.2604	0.082728	1.7595	HMDB0000094	Citric acid	[M-H]-	9	Tricarboxylic acids and derivatives	Endogenous|Food|Synthetic|Biological	C00158	map00020; map00250; map00630; map00720; map00997; map01053; map01060; map01061; map01062; map01063; map01064; map01065; map01066; map01070; map01100; map01110; map01120; map01200; map01210; map01230; map01240; map02020; map04742; map04922; map05230	Citrate cycle (TCA cycle); Alanine, aspartate and glutamate metabolism; Glyoxylate and dicarboxylate metabolism; Carbon fixation pathways in prokaryotes; Biosynthesis of various secondary metabolites - part 3; Biosynthesis of siderophore group nonribosomal peptides; Biosynthesis of plant secondary metabolites; Biosynthesis of phenylpropanoids; Biosynthesis of terpenoids and steroids; Biosynthesis of alkaloids derived from shikimate pathway; Biosynthesis of alkaloids derived from ornithine, lysine and nicotinic acid; Biosynthesis of alkaloids derived from histidine and purine; Biosynthesis of alkaloids derived from terpenoid and polyketide; Biosynthesis of plant hormones; Metabolic pathways; Biosynthesis of secondary metabolites; Microbial metabolism in diverse environments; Carbon metabolism; 2-Oxocarboxylic acid metabolism; Biosynthesis of amino acids; Biosynthesis of cofactors; Two-component system; Taste transduction; Glucagon signaling pathway; Central carbon metabolism in cancer
212.0413	4.2951	2.1027	0.016832	2.0793	HMDB0001511	Phosphocreatine	[M+H]+	8	Amino acids, peptides, and analogues	Endogenous	C02305	map00330; map01100	Arginine and proline metabolism; Metabolic pathways
217.1039	0.3095	-1.692	0.074128	1.7914	HMDB0029027	Prolyl-Threonine	[M+H]+	66	Amino acids, peptides, and analogues	Endogenous	-	-	-

239.1487	3.0514	1.6095	0.002226	2.2403	HMDB0139940	N-(3-aminopropyl)-3-(3,4-dihydroxyphenyl)propanimidic acid	[M+H]+	41	Benzenediols	Endogenous	-	-	-
268.1042	2.1692	1.1172	0.079006	1.7731	HMDB0000050	Adenosine	[M+H]+	0	-	Endogenous|Food|Synthetic|Biological	C00212	map00230; map01100; map02010; map04022; map04024; map04071; map04080; map04270; map04923; map04924; map05012; map05032; map05034	Purine metabolism; Metabolic pathways; ABC transporters; cGMP-PKG signaling pathway; cAMP signaling pathway; Sphingolipid signaling pathway; Neuroactive ligand-receptor interaction; Vascular smooth muscle contraction; Regulation of lipolysis in adipocytes; Renin secretion; Parkinson disease; Morphine addiction; Alcoholism
337.2046	0.42024	-1.2507	0.055779	1.8655	HMDB0040566	[6]-Gingerdiol 3-acetate	[M-H]-	8	Fatty alcohol esters	Food|Endogenous|Biological	-	-	-
341.3064	0.28176	-1.8275	0.070702	1.8045	HMDB0032476	Polyoxyethylene (600) monoricinoleate	[M+H]+	4	Fatty alcohols	Endogenous|Food|Biological	-	-	-
400.345	0.23881	-2.0661	0.021729	2.0443	HMDB0000222	L-Palmitoylcarnitine	[M+H]+	7	Fatty acid esters	Endogenous|Food|Biological	C02990	map00071; map01212	Fatty acid degradation; Fatty acid metabolism
417.2988	2.3256	1.2176	0.06897	1.8113	HMDB0036886	beta-Carotinal	[M+H]+	39	Triterpenoids	Endogenous|Food|Biological	-	-	-
425.125	2.3924	1.2585	0.090263	1.7328	HMDB0003556	Chitobiose	[M-H]-	38	Carbohydrates and carbohydrate conjugates	Endogenous	C01674	map00520; map01100; map02010; map02060	Amino sugar and nucleotide sugar metabolism; Metabolic pathways; ABC transporters; Phosphotransferase system (PTS)
455.0973	2.9588	1.565	0.041847	1.9298	HMDB0001520	Flavin mononucleotide	[M-H]-	0	-	Endogenous|Food|Biological	C00061	map00190; map00740; map00997; map01057; map01100; map01110; map01240; map04977	Oxidative phosphorylation; Riboflavin metabolism; Biosynthesis of various secondary metabolites - part 3; Biosynthesis of type II polyketide products; Metabolic pathways; Biosynthesis of secondary metabolites; Biosynthesis of cofactors; Vitamin digestion and absorption

485.2707	0.24874	-2.0073	0.068811	1.8119	HMDB0011156	PA (O-20:4 (5Z,8Z, 11Z,14Z)/ 2:0)	[M-H]-	7	Glycero-phos-phates	Endog-enous| Food| Biological	-	-	-
494.3191	0.46812	-1.095	0.074051	1.7917	HMDB0010383	LysoPC (16:1 (9Z)/0:0)	[M+H]+	10	Glycero-phospho-cholines	Endog-enous| Food| Biological	C04230	map00564; map05231	Glycerophospholipid metabolism; Choline metabolism in cancer
504.3039	0.40545	-1.3024	0.093119	1.723	HMDB0010381	LysoPC (15:0/0:0)	[M+Na]+	4	Glycero-phospho-cholines	Endog-enous| Food| Biological	C04230	map00564; map05231	Glycerophospholipid metabolism; Choline metabolism in cancer
505.3484	21.317	4.4139	0.06939	1.8096	HMDB0032111	Adlupone	[M+Na]+	39	Carbonyl com-pounds	Endog-enous| Food	-	-	-
512.2956	0.43086	-1.2147	0.088452	1.7392	HMDB0002639	Sulfolithocholyl-glycine	[M-H]-	53	Bile acids, alcohols and deriva-tives	Endog-enous| Food| Biological	C11301	-	-
539.3611	0.19266	-2.3759	0.061443	1.8416	HMDB0002815	LysoPC (18:1 (9Z)/ 0:0)	[M+NH4]+	39	Glycero-phospho-cholines	Endog-enous| Food| Biological	-	-	-
539.5361	2.953	1.5622	0.050784	1.8876	HMDB0041080	9-Hydroxytridec-yl docosanoate	[M+H]+	7	Fatty acid esters	Food| Endog-enous| Biological	-	-	-
540.329	0.48503	-1.0439	0.076519	1.7824	HMDB0010397	LysoPC (20:5 (5Z,8Z, 11Z,14Z, 17Z)/0:0)	[M-H]-	36	Glycero-phospho-cholines	Endog-enous| Food| Biological	C04230	map00564; map05231	Glycerophospholipid metabolism; Choline metabolism in cancer
544.3388	0.30709	-1.7033	0.009198	2.1457	HMDB0010395	LysoPC (20:4 (5Z,8Z, 11Z,14Z)/ 0:0)	[M+H]+	2	Glycero-phospho-cholines	Endog-enous| Food| Biological	C04230	map00564; map05231	Glycerophospholipid metabolism; Choline metabolism in cancer
553.3832	2.6147	1.3866	0.048019	1.9002	HMDB0033632	Furohyperforin	[M+H]+	10	Monoter-penoids	Endog-enous| Food| Biological	-	-	-

565.0451	4.2373	2.0831	0.090551	1.7318	HMDB0000286	Uridine diphosphate glucose	[M-H]-	5	Pyrimidine nucleotide sugars	Endogenous|Food|Biological	C00029	map00040; map00052; map00053; map00240; map00500; map00520; map00524; map00541; map00561; map00908; map01051; map01060; map01100; map01110; map01240	Pentose and glucuronate interconversions; Galactose metabolism; Ascorbate and aldarate metabolism; Pyrimidine metabolism; Starch and sucrose metabolism; Amino sugar and nucleotide sugar metabolism; Neomycin, kanamycin and gentamicin biosynthesis; O-Antigen nucleotide sugar biosynthesis; Glycerolipid metabolism; Zeatin biosynthesis; Biosynthesis of ansamycins; Biosynthesis of plant secondary metabolites; Metabolic pathways; Biosynthesis of secondary metabolites; Biosynthesis of cofactors
570.3544	0.2986	-1.7437	0.007826	2.1603	HMDB0010402	LysoPC (22:5 (4Z,7Z, 10Z,13Z, 16Z)/0:0)	[M+H]+	2	Glycerophosphocholines	Endogenous|Food|Biological	C04230	map00564; map05231	Glycerophospholipid metabolism; Choline metabolism in cancer
590.3433	0.23028	-2.1185	0.044356	1.9175	HMDB0029334	Nummularine B	[M-H]-	76	Amino acids, peptides, and analogues	Endogenous|Food|Biological	-	-	-
594.2841	0.47768	-1.0659	0.054713	1.8701	HMDB0002581	Taurocholic acid 3-sulfate	[M-H]-	72	Bile acids, alcohols and derivatives	Endogenous|Food|Biological	-	-	-
609.5544	2.1783	1.1232	0.034531	1.9675	HMDB0060057	CE (15:0)	[M-H]-	12	Steroid esters	Food|Endogenous|Biological	-	-	-
623.5026	4.8138	2.2672	0.013259	2.108	HMDB0029958	Asitribin	[M+H]+	23	Fatty alcohols	Food|Endogenous|Biological	-	-	-
625.3451	5.122	2.3567	0.084958	1.7515	HMDB0034091	Ponasteroside A	[M-H]-	23	Steroidal glycosides	Endogenous|Food|Biological	-	-	-
645.2995	0.47979	-1.0595	0.082563	1.7601	HMDB0030736	Capsianoside IV	[M+H]+	75	Fatty acyl glycosides	Endogenous|Food|Biological	-	-	-
648.4355	2.8519	1.5119	0.023982	2.0294	HMDB0008856	PE (14:1 (9Z)/ 15:0)	[M+H]+	38	Glycerophosphoethanolamines	Endogenous|Food|Biological	-	-	-

662.1056	15.383	3.9432	0.040327	1.9373	HMDB0000902	NAD	[M-H]-	6	-	Endogenous	C00003	map00190; map00730; map00760; map00983; map01100; map01240; map04152; map04211; map04212; map04925; map04977	Oxidative phosphorylation; Thiamine metabolism; Nicotinate and nicotinamide metabolism; Drug metabolism - other enzymes; Metabolic pathways; Biosynthesis of cofactors; AMPK signaling pathway; Longevity regulating pathway; Longevity regulating pathway - worm; Aldosterone synthesis and secretion; Vitamin digestion and absorption
675.5414	0.37932	-1.3985	0.085516	1.7495	HMDB0012097	SM (d18:1/14:0)	[M+H]+	3	Phosphosphingolipids	Endogenous|Food|Biological	-	-	-
688.5332	2.9021	1.5371	0.037444	1.9521	HMDB0114836	PA (16:0/18:3 (6Z,9Z,12Z))	[M+NH4]+	61	Glycerophosphates	Food|Endogenous|Biological	-	-	-
694.5228	0.27354	-1.8702	0.045556	1.9118	HMDB0012321	Galactosylceramide (d18:1/14:0)	[M+Na]+	0	Glycosphingolipids	Endogenous|Food|Biological	C02686	-	-
696.5389	3.1372	1.6495	0.02101	2.0491	HMDB0009213	PE (18:4 (6Z,9Z,12Z,15Z)/P-16:0)	[M+H]+	61	Glycerophosphoethanolamines	Endogenous|Food|Biological	-	-	-
703.5717	2.5709	1.3623	0.027878	2.0053	HMDB0010169	SM (d18:1/16:0)	[M+H]+	5	Phosphosphingolipids	Endogenous|Food|Biological	-	-	-
722.5062	0.38759	-1.3674	0.088715	1.7382	HMDB0009215	PE (18:4 (6Z,9Z,12Z,15Z)/P-18:1 (11Z))	[M+H]+	8	Glycerophosphoethanolamines	Endogenous|Food|Biological	-	-	-
730.5422	0.25198	-1.9886	0.002753	2.2301	HMDB0007874	PC (14:0/18:2 (9Z,12Z))	[M+H]+	5	Glycerophosphocholines	Endogenous|Food|Biological	-	-	-
732.5532	0.25701	-1.9601	0.014425	2.0983	HMDB0007872	PC (14:0/18:1 (11Z))	[M+H]+	1	Glycerophosphocholines	Endogenous|Food|Biological	-	-	-

736.4773	0.47898	-1.0619	0.073823	1.7925	HMDB0008847	PE (14:0/ 22:6 (4Z, 7Z,10Z, 13Z, 16Z,19Z))	[M+H]+	19	Glycero-phospho-ethanol-amines	Endog-enous| Food| Biological	C00350	map00563; map00564; map01100; map01110; map04136; map04138; map04140; map04723; map05130; map05167	Glycosylphosphatidylinositol (GPI)-anchor biosynthesis; Glycerophospholipid metabo-lism; Metabolic pathways; Biosynthesis of secondary metabolites; Autophagy - other; Autophagy - yeast; Autophagy - animal; Retro-grade endocannabinoid signaling; Pathogenic Escherichia coli infection; Kaposi sarcoma-associated herpesvirus infection
744.5588	0.21351	-2.2276	0.041524	1.9314	HMDB0007938	PC (15:0/ 18:1 (11Z))	[M-H]-	5	Glycero-phospho-cholines	Endog-enous| Food| Biological	C00157	map00564; map00590; map00591; map00592; map01100; map01110; map04723; map05231	Glycerophospholipid metabolism; Arachidonic acid metabolism; Linoleic acid metabolism; alpha-Linolenic acid metabolism; Metabolic pathways; Biosynthesis of secondary metabo-lites; Retrograde endocannabinoid signaling; Choline metabolism in cancer
746.5048	0.38267	-1.3858	0.009179	2.1459	HMDB0112425	PS (18:2 (9Z,12Z)/ 15:0)	[M+H]+	11	Glycero-phospho-serines	Food| Endog-enous| Biological	-	-	-
748.5233	2.1143	1.0802	0.084229	1.7541	HMDB0005780	PE (P-16:0/ 22:6 (4Z,7Z, 10Z,13Z, 16Z,19Z))	[M+H]+	6	Glycero-phospho-ethanol-amines	Endog-enous| Food| Biological	C00350	map00563; map00564; map01100; map01110; map04136; map04138; map04140; map04723; map05130; map05167	Glycosylphosphatidylinositol (GPI)-anchor biosynthesis; Glycerophospholipid metabo-lism; Metabolic pathways; Biosynthesis of secondary metabolites; Autophagy - other; Autophagy - yeast; Autophagy - animal; Retro-grade endocannabinoid signaling; Pathogenic Escherichia coli infection; Kaposi sarcoma-associated herpesvirus infection
749.524	0.47217	-1.0826	0.037025	1.9543	HMDB0030449	20-Deoxynara-sin	[M+H]+	6	Terpene glyco-sides	Endog-enous| Food| Biological	-	-	-
769.5023	2.3254	1.2175	0.019433	2.0601	HMDB0010575	PG (16:0/ 18:2 (9Z,12Z))	[M+Na]+	4	Glycero-phospho-glycerols	Endog-enous| Food| Biological	-	-	-
772.5854	0.27789	-1.8474	0.082765	1.7594	HMDB0007946	PC (15:0/ 20:2 (11Z,14Z))	[M+H]+	0	Glycero-phospho-cholines	Endog-enous| Food| Biological	-	-	-
776.5609	2.6157	1.3872	0.034865	1.9657	HMDB0009644	PE (22:5 (4Z,7Z, 10Z,13Z, 16Z)/ P-18:1 (11Z))	[M+H]+	3	Glycero-phospho-ethanol-amines	Endog-enous| Food| Biological	-	-	-

779.53	0.16474	-2.6018	0.054714	1.8701	HMDB0115112	PA (20:1(11Z)/ 22:4 (7Z,10Z, 13Z,16Z))	[M+H]+	37	Glycero-phos-phates	Food| Endog-enous| Biological	-	-	-
780.5078	0.43494	-1.2011	0.026025	2.0166	HMDB0012313	3-O-Sulfogalac-tosylceramide (d18:1/ 16:0)	[M+H]+	27	Glyco-sphingo-lipids	Endog-enous| Food| Biological	C06125	map00600; map01100	Sphingolipid metabolism; Metabolic pathways
780.5469	2.9935	1.5819	0.01826	2.0686	HMDB0007890	PC (14:0/ 22:5 (4Z,7Z, 10Z,13Z, 16Z))	[M+H]+	9	Glycero-phospho-cholines	Endog-enous| Food| Biological	-	-	-
794.5675	0.40669	-1.298	0.015275	2.0914	HMDB0007956	PC (15:0/ 22:5 (4Z,7Z, 10Z, 13Z,16Z))	[M+H]+	3	Glycero-phospho-cholines	Endog-enous| Food| Biological	-	-	-
797.525	0.27068	-1.8854	0.033184	1.9749	HMDB0010581	PG (16:0/ 22:4 (7Z,10Z, 13Z,16Z))	[M-H]-	11	Glycero-phospho-glycerols	Endog-enous| Food| Biological	-	-	-
804.548	0.41074	-1.2837	0.010467	2.1332	HMDB0007889	PC (14:0/ 22:4 (7Z,10Z, 13Z,16Z))	[M+Na]+	4	Glycero-phospho-cholines	Endog-enous| Food| Biological	-	-	-
806.5619	0.27614	-1.8565	0.032865	1.9766	HMDB0004866	LacCer (d18:1/ 12:0)	[M+H]+	1	-	Endog-enous| Food| Biological	-	-	-
825.5572	0.22222	-2.1699	0.033226	1.9746	HMDB0061422	PC (DiMe (9,3)/ MonoMe (11,3))	[M+H]+	7	Glycero-phospho-cholines	Endog-enous| Food| Biological	-	-	-
826.5584	8.1981	3.0353	0.001533	2.2558	HMDB0008189	PC (18:3(6Z, 9Z,12Z)/ 22:6 (4Z,7Z, 10Z,13Z, 16Z,19Z))	[M-H]-	23	Glycero-phospho-cholines	Endog-enous| Food| Biological	-	-	-
840.5239	0.29165	-1.7777	0.057932	1.8563	HMDB0061555	PS (DiMe (11,3)/ DiMe (9,3))	[M+H]+	26	Glycero-phospho-serines	Endog-enous| Food| Biological	-	-	-
854.6698	0.33573	-1.5746	0.068492	1.8131	HMDB0009278	PE (20:1 (11Z)/ 24:1 (15Z))	[M-H]-	6	Glycero-phospho-ethanol-amines	Endog-enous| Food| Biological	-	-	-

865.5056	5.0623	2.3398	0.08721	1.7435	HMDB0116605	PG (22:6 (4Z,7Z, 10Z,13Z, 16Z,19Z)/ 22:6 (4Z,7Z, 10Z,13Z, 16Z,19Z))	[M-H]-	4	Glycero-phospho-glycerols	Food| Endog-enous| Biological	-	-	-
889.5481	0.46291	-1.1112	0.05578	1.8655	HMDB0009785	PI (16:0/ 20:0)	[M+Na]+	33	Glycero-phospho-inositols	Endog-enous| Food| Biological	-	-	-
913.5269	0.40101	-1.3183	0.078158	1.7763	HMDB0034650	Soyasaponin II	[M+H]+	12	Terpene glyco-sides	Endog-enous| Food| Biological	C12081	-	-
952.5933	0.2021	-2.3068	0.037455	1.952	HMDB0061563	PS (DiMe (11,5)/ DiMe (13,5))	[M+H]+	36	Glycero-phospho-serines	Endog-enous| Food| Biological	-	-	-
1151.703	0.1284	-2.9613	0.069028	1.811	HMDB0004844	Ganglioside GM3 (d18:1/ 16:0)	[M-H]-	2	Glyco-sphingo-lipids	Endog-enous| Food| Biological	C04730	-	-